



Entropy generation analysis of a nanofluid flow in MHD porous microchannel with hydrodynamic slip and thermal radiation



Guillermo Ibáñez*, Aracely López, Joel Pantoja, Joel Moreira

Universidad de Ciencias y Artes de Chiapas, Libramiento Norte Poniente No. 1150, Col. Lajas Maciel, Tuxtla Gutiérrez, Chiapas C.P. 29039, Mexico

ARTICLE INFO

Article history:

Received 20 November 2015
Received in revised form 22 April 2016
Accepted 23 April 2016
Available online 6 May 2016

Keywords:

MHD nanofluid flow
Porous microchannel
Entropy generation

ABSTRACT

Combined effects of hydrodynamic slip, magnetic field, suction/injection, thermal radiation, nanoparticle volume fraction and convective boundary conditions on the heat transfer and global entropy generation in a viscous electrically conducting nanofluid flow through a microchannel with permeable plates are studied. Analytical solutions of the momentum and the energy equations are obtained in closed form. Particularly, considering the radiative term, joule heating and viscous dissipation in the energy equation, the temperature field of the nanofluid is derived analytically. Influences of pertinent parameters on global entropy generation are discussed in detail and depicted graphically. Analysis of our results indicates that entropy generation minimization can be achieved by appropriate combination of the geometrical and physical parameters of the system. It is possible to determine optimum values of radiation parameter, nanoparticle volume fraction, Hartmann and Biot numbers which lead to a minimum global entropy generation rate. The Nusselt number is also calculated and explored for different conditions. Optimum values of nanoparticle volume fraction and magnetic field strength that maximize heat transfer are derived.

© 2016 Elsevier Ltd. All rights reserved.

1. Introduction

In recent years, microfluidics become an important area of research. Analysis of heat and fluid flow at microscale is of great importance for application in micro heat exchanger systems. Particularly, study of steady laminar forced convection fluid flow through parallel plates in a microchannel has many significant applications in engineering. Starting from the design of cooling systems for microelectronic devices to various microscale electromechanical systems, such as MHD micropumps, micro turbines and fuel cells, this type of geometry can be observed. In this context, nanofluids in microchannels have gained much attention because the effective thermal conductivity of conventional fluids, such as water and engine oil, increases remarkably with the addition of nanoscale metallic particles with high thermal conductivity. Various investigations have been performed to explore the potential of nanofluids in heat transfer applications [1–7]. In particular, the study of nanofluid flow in microchannels has been reported in the literature [8–13]. Mohammed et al. [8] and Salman et al. [9] found that nanofluids in the microchannel heat exchangers

dramatically enhance cooling rate compared with conventional water cooled microchannel heat exchangers.

In the present study optimization of magnetohydrodynamic (MHD) flow of a nanofluid in a porous microchannel using the entropy generation minimization method (EGM) and considering combined effects of slip flow, suction/injection, thermal radiation and convective heat transfer is carried out. Reducing entropy generation of nanofluid motion through porous MHD channels can have a beneficial impact on the input power required to achieve both desired heat exchange and mass flow rates. Therefore, in energy optimization problems and design of many heat removal engineering devices, it is imperative to determine factors that contribute to entropy generation in order to minimize their effects and maximize available work. A review on entropy generation of nanofluids shows that suspension of nanoparticles in a conventional fluid can be very beneficial in decreasing of the entropy generation [6]. Here, hydrodynamic slip is considered on the walls of the microchannel because it is well known that in some applications in microfluidic and nanofluidic devices where the surface to volume ratio is large, slip flow conditions are more typical and slip boundary condition is usually used for the velocity field [14–17]. Moreover, entropy analysis of ordinary fluid flow through a porous channel with hydrodynamic slip [18–22] is of interest due to wide applications in various fields such as diffusion technology, transpiration cooling, hemodialysis processes, flow control in nuclear

* Corresponding author. Tel.: +52 01 961 6170440x4200; fax: +52 01 961 6170440x4231.

E-mail addresses: guibdu@gmail.com (G. Ibáñez), alpezib@hotmail.com (A. López), jpe2005@gmail.com (J. Pantoja), jmoreira23@yahoo.com.mx (J. Moreira).

reactors and certain problems of the movement of conductive physiological fluids. In particular, some works have addressed the analysis of entropy generation in porous channels considering MHD flow of a nanofluid [23–25]. In these papers the entropy generation rate was calculated but effects of thermal radiation on heat transfer and entropy generation rate were not considered.

Investigations of electromagnetic flow of nanofluids with radiation effects are reported by various authors [26–31]. Zhang et al. [26] performed an analytical study of MHD flow of a nanofluid in a porous medium with variable surface heat flux and chemical reaction using the differential transform base functions method (DTM-BF). They found that magnetic field and radiation have significant effects on velocity and temperature fields. Pal and Mandal [27] studied hydromagnetic convective-radiative boundary layer flow of nanofluid induced by a nonlinear vertical stretching/shrinking sheet with viscous and ohmic dissipation. The governing equations were solved numerically using a fifth order Runge–Kutta–Fehlberg method with shooting technique. The results revealed that heat transfer at the boundary layer increases with increasing nanoparticle volume fraction. Ganesh et al. [28] presented analytical and numerical studies on hydromagnetic flow of a nanofluid over a stretching sheet with thermal radiation. The dimensionless governing equations are solved analytically using hypergeometric functions and numerically by the Nachtsheim–Swigert shooting iteration technique together with the fourth order Runge–Kutta integration scheme. They analyzed the influence of pertinent parameters such as magnetic parameter, solid volume fraction of nanoparticles and radiation parameter. Their results indicated that when the radiation parameter increases the thermal boundary layer of the nanofluid decreases. Mushtaq et al. [29] investigated radiation effects in MHD flow of a viscous nanofluid due to solar energy. The resulting differential equations were solved numerically using a fourth-fifth order Runge–Kutta method (RK45) with shooting technique. The analysis of their results showed that the temperature and the wall temperature gradient increase with the radiation parameter. Nandy et al. [30] investigated effects of magnetic field and thermal radiation on stagnation flow and heat transfer of a nanofluid over a shrinking surface. A similarity transformation was used to transform the governing partial differential equations to a system of nonlinear ordinary differential equations which were solved numerically using a shooting technique. They concluded that the magnetic parameter has a strong influence over velocity and temperature. Rahman et al. [31] investigated the role of a convective surface on heat transfer of water-based nanofluids in the presence of thermal radiation. The numerical results were obtained using a fourth-fifth order Runge–Kutta method (RK45). They showed that the rate of heat transfer in a nanofluid in the presence of thermal radiation depends significantly on the surface convection parameter. In the above studies thermal radiation effects were considered but entropy generation was not calculated.

Recent works have addressed analysis of entropy generation in nanofluids with inclusion of thermal radiation [32–37]. Habibi et al. [32] investigated entropy generation of nanofluid flow in an MHD channel formed by two parallel isothermal plates considering thermal radiation effect and using air as main fluid with Al_2O_3 , Cu and Ti nanoparticles. It was found that there is a minimum value for the total entropy generation rate versus the radiation parameter. Mahmoodi and Kandelousi [33] studied heat transfer and entropy generation of kerosene-alumina nanofluid in a channel with thermal radiation. Differential Transform Method was utilized to solve the governing equations. Their results showed that the Bejan number has a direct relationship with the radiation parameter. In [34], a semi-analytical study of hydrothermal behavior and entropy generation of kerosene-alumina nanofluid in a regenerative cooling channel considering thermal radiation was performed. The results indicated that entropy generation is a

decreasing function of the radiation parameter. Torabi and Aziz [35] considered hollow cylindrical geometries with radiation effect. To solve the energy equation and obtain the entropy generation, the differential transform method was applied. Torabi and Zhang [36] evaluated both homogenous and functionally graded slabs with internal heat generation and radiation effects from the second law of thermodynamics point of view. In [37], temperature distribution, and local and total entropy generation rates within two-layer composite walls using conjugate convection and radiation boundary conditions were investigated. Although the entropy generation rate was calculated in these investigations, combined effects of hydrodynamic slip, suction/injection, thermal radiation, volume fraction of solid nanoparticles and convective boundary conditions were not considered.

In the present contribution, recent work of Ibáñez [22] is extended to include effects of thermal radiation and solid volume fraction of nanoparticles on both heat transfer and entropy generation in an MHD porous microchannel. The main fluid is water with Al_2O_3 nanoparticles. Exact analytic solutions are presented for velocity and temperature fields in the nanofluid. It is noted that the present solution reduces to previous results [22] by taking the radiation parameter (Rd) and the solid volume fraction of nanoparticles equal to zero which provides a useful mathematical check. Here, the behavior of the local Nusselt number is also explored. Optimum values of the nanoparticle volume fraction and Hartmann number that maximize heat transfer are derived.

Although there exist a large number of studies in the literature dealing with MHD heat transfer in nanofluid flow through a microchannel under different boundary and geometrical configurations, most of these studies do not take into account simultaneously all the effects considered in the present work and their analysis is mainly focused on local entropy generation. In addition, optimum operation conditions, namely optimum values of entropy generation rate and Nusselt number are not always obtained. In our study optimum conditions where the irreversibilities are minimum and heat transfer is maximum are obtained for the system, therefore the fundamental contributions compared with the existing literature are: (a) The local and global entropy production in water- Al_2O_3 nanofluid flow through a microchannel is determined from the solution of heat transfer problem considering thermal radiation, hydrodynamic slip, suction/injection, magnetic field, nanoparticle volume fraction and convective heat transfer effects, simultaneously, (b) All relevant design parameters for the system are optimized by minimizing the global entropy generation. Particularly, optimum values of the radiation parameter and the nanoparticle volume fraction that minimize entropy generation are found, (c) Optimum values of nanoparticle volume fraction and magnetic field strength that maximize heat transfer are obtained and (d) Effects of solid volume fraction of nanoparticles on optimum values of some other parameters in which entropy is minimum are analyzed.

In the following sections, the problem is formulated, analyzed, solved and discussed. Section 2 consists of the transport problem analysis which contains the momentum and energy balance equations and their solutions. Section 3 contains the determination of the entropy generation rate and the Nusselt number for this problem, and graphical representation of results and their discussion. Section 4 contains the concluding remarks.

2. The model fluid and the governing equations

We consider steady fully developed flow of a viscous MHD nanofluid through a microchannel with two horizontal parallel porous plates separated by a distance a in the presence of a constant longitudinal pressure gradient dp/dx' and under a uniform

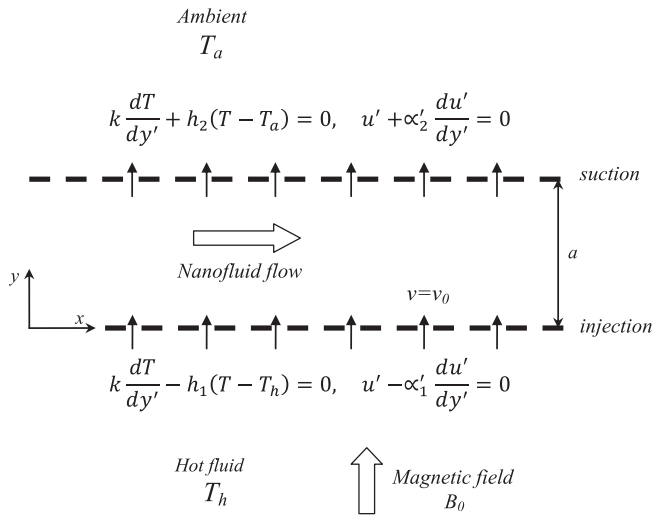


Fig. 1. Geometry of the flow.

transverse magnetic field B_0 . The upper plate is located at $y' = a$ and the lower plate is at $y' = 0, y'$, denoting the transversal coordinate. It is assumed that the parallel plates are infinite so that the velocity and temperature profiles are fully developed, also the fluid is injected uniformly into the microchannel at the lower plate and fluid suction occurs at the upper plate. The microchannel lower plate exchanges heat by convection with a hot fluid with temperature T_h while the upper plate is in contact with the ambient temperature. For the solution of the momentum balance equation we assume that the velocity satisfies the slip condition at the plates. In turn, the heat transfer equation is solved using convective boundary conditions and considering thermal radiation flux, viscous dissipation and Joule heating. A schematic view of the MHD porous microchannel is shown in Fig. 1.

2.1. Velocity and temperature fields

Given the previous assumptions the momentum equation is

$$\rho_{nf} v_0 \frac{du'}{dy'} = -\frac{dp}{dx'} + \eta_{nf} \frac{d^2 u'}{dy'^2} - \sigma_{nf} B_0^2 u'. \tag{1}$$

Let us assume that the surface roughness of each plate is in general different. Then, the slip lengths, although taken to be constant, do not have the same value on both plates. Therefore, Eq. (1) must satisfy the boundary conditions

$$u' - \alpha_1 \frac{du'}{dy'} = 0, \quad \text{at } y' = 0, \tag{2}$$

$$u' + \alpha_2 \frac{du'}{dy'} = 0, \quad \text{at } y' = a, \tag{3}$$

where v_0 is the uniform suction/injection velocity at the microchannel plates. Here, η_{nf} is the dynamic viscosity, σ_{nf} is the electrical conductivity and ρ_{nf} is the density of the nanofluid, while α_1 and α_2 are the slip lengths of the lower and upper plates, respectively.

The energy balance equation in the fluid reduces to [26]

$$(\rho C)_{nf} v_0 \frac{dT}{dy'} = k_{nf} \frac{\partial^2 T}{\partial y'^2} + \eta_{nf} \left(\frac{du'}{dy'} \right)^2 + \sigma_{nf} B_0^2 u'^2 - \frac{\partial q_r}{\partial y'}. \tag{4}$$

The boundary conditions that Eq. (4) must satisfy are

$$k_{nf} \frac{dT}{dy'} - h_1(T - T_h) = 0, \quad \text{at } y' = 0, \tag{5}$$

$$k_{nf} \frac{dT}{dy'} + h_2(T - T_a) = 0, \quad \text{at } y' = a, \tag{6}$$

where T is the nanofluid temperature, T_h is the hot fluid temperature, T_a is the ambient temperature, k_{nf} and C_{nf} are the thermal conductivity and heat capacitance of nanofluid, respectively, while h_1 and h_2 are the convective heat transfer coefficients for each plate. The third term on the right-hand side of Eq. (4) is the Joule dissipation described in terms of Ohm's law and the fourth term takes into account heat flux due to thermal radiation.

The thermal radiation flux considering diffusion method of radiation transfer can be written as follows (Rosseland diffusion approximation):

$$q_r = -\frac{\sigma}{3k^*} T_b^3 \frac{dT}{dy'}, \tag{7}$$

where T_b is the bulk temperature that is the average temperature of the nanofluid, σ is the Stefan–Boltzmann constant and k^* is the Rosseland mean absorption coefficient.

Introducing dimensionless variables

$$u = \frac{\rho_f a u'}{\eta_f}, \quad y = \frac{y'}{a}, \quad \alpha_1 = \frac{\alpha'_1}{a}, \quad \alpha_2 = \frac{\alpha'_2}{a} \quad \text{and} \quad \theta = \frac{T - T_a}{T_h - T_a},$$

Eqs. (1)–(6) become

$$\frac{\rho_{nf}}{\rho_f} Re \frac{du}{dy} = P + \frac{\eta_{nf}}{\eta_f} \frac{d^2 u}{dy^2} - \frac{\sigma_{nf}}{\sigma_f} M^2 u, \tag{8}$$

$$u - \alpha_1 \frac{du}{dy} = 0, \quad \text{at } y = 0, \tag{9}$$

$$u + \alpha_2 \frac{du}{dy} = 0, \quad \text{at } y = 1, \tag{10}$$

$$\frac{(\rho C)_{nf}}{(\rho C)_f} Pe \frac{d\theta}{dy} = \left(\frac{k_{nf}}{k_f} + Rd \right) \frac{\partial^2 \theta}{\partial y^2} + EcPr \left[\frac{\eta_{nf}}{\eta_f} \left(\frac{du}{dy} \right)^2 + \frac{\sigma_{nf}}{\sigma_f} M^2 u^2 \right], \tag{11}$$

$$\frac{k_{nf}}{k_f} \frac{d\theta}{dy} - Bi_1(\theta - 1) = 0, \quad \text{at } y = 0, \tag{12}$$

$$\frac{k_{nf}}{k_f} \frac{d\theta}{dy} + Bi_2(\theta) = 0, \quad \text{at } y = 1, \tag{13}$$

where

$$\frac{\rho_{nf}}{\rho_f} = (1 - \phi) + \phi \frac{\rho_s}{\rho_f}, \tag{14}$$

$$\frac{(\rho C)_{nf}}{(\rho C)_f} = (1 - \phi) + \phi \frac{(\rho C)_s}{(\rho C)_f}, \tag{15}$$

$$\frac{\eta_{nf}}{\eta_f} = \frac{1}{(1 - \phi)^{2.5}}, \tag{16}$$

$$\frac{k_{nf}}{k_f} = \frac{k_s + 2k_f - 2\phi(k_f - k_s)}{k_s + 2k_f + \phi(k_f - k_s)}, \tag{17}$$

$$\frac{\sigma_{nf}}{\sigma_f} = 1 + \frac{3\phi(\frac{\sigma_s}{\sigma_f} - 1)}{(\frac{\sigma_s}{\sigma_f} + 2) - \phi(\frac{\sigma_s}{\sigma_f} - 1)}. \tag{18}$$

Here, ϕ is the solid volume fraction of nanoparticles (Al_2O_3), $\rho_f, (\rho C)_f, \eta_f, k_f$ and σ_f are the density, heat capacitance, dynamic viscosity, thermal conductivity and electrical conductivity of the base fluid (water), respectively, while $\rho_s, (\rho C)_s, \eta_s, k_s$ and σ_s are

the density, heat capacitance, dynamic viscosity, thermal conductivity and electrical conductivity of the nanoparticles, respectively. $P = \frac{\alpha^2 \rho_f}{\eta_f^2} (-\frac{dp}{dx})$ is the pressure gradient parameter, $Re = v_0 \alpha \rho_f / \eta_f$ is the Reynolds number, $Pr = \eta_f C_f / k_f$ is the Prandtl number, $Ec = v_0^2 / C_f (T_h - T_a)$ is the Eckert number, $Pe = RePr$ is the Peclet number, $Rd = \frac{16\sigma T_b^3}{3k k_f}$ is the radiation parameter, $M = B_0 a \sqrt{\sigma_f / \eta_f}$ is the Hartmann number and $Bi_i = ah_i / k_f$ is the Biot number for each plate. Subindices $i = 1, 2$ refer to the lower and upper plates, respectively.

2.2. Results

The solution to Eq. (8) with the boundary conditions (9 and 10) is given by

$$u = F_3 + e^{\frac{F_1}{2}y} (C_1 \sinh[Ay] + C_2 \cosh[Ay]), \tag{19}$$

where

$$C_1 = \frac{F_3}{A\alpha_1} \left[1 - \frac{(A\alpha_1 + F_4)(2 - \alpha_1 F_1)}{(2 - \alpha_1 F_1)F_4 + 2A\alpha_1 F_5} \right],$$

$$C_2 = \frac{-2F_3(A\alpha_1 + F_4)}{(2 - \alpha_1 F_1)F_4 + 2A\alpha_1 F_5},$$

$$A = \sqrt{\frac{F_1^2}{4} + F_2},$$

$$F_1 = \frac{\eta_f}{\eta_{nf}} \frac{\rho_{nf}}{\rho_f} Re,$$

$$F_2 = \frac{\eta_f}{\eta_{nf}} \frac{\sigma_{nf}}{\sigma_f} M^2,$$

$$F_3 = \frac{\eta_f P}{\eta_{nf} M^2},$$

$$F_4 = e^{\frac{F_1}{2}} \left[\sinh[A] \left(1 + \alpha_2 \frac{F_1}{2} \right) + A\alpha_2 \cosh[A] \right],$$

$$F_5 = e^{\frac{F_1}{2}} \left[\cosh[A] \left(1 + \alpha_2 \frac{F_1}{2} \right) + A\alpha_2 \sinh[A] \right].$$

In Fig. 2 the velocity profile is shown for different values of slip parameter, α , and Hartmann number, M , for $P = 1, Re = 1$ and $\phi = 0.1$. It is evident that the velocity increases with the slip parameter, while the main effect of the Hartmann number on the flow velocity is to flatten the profile, decreasing the velocity. This can be attributed to the presence of Lorentz force acting as a resistance to the flow. With $\alpha_1 = \alpha_2 = 0$, the velocity profile given by Eq. (19) reduces to the result of [38] in the non-slip flow case through an MHD porous channel, while when the volume fraction of nanoparticles, ϕ , is equal to zero, the velocity profile reduces to the result of [22].

In Fig. 3, effects of the volume fraction of nanoparticles and Reynolds number on the velocity profile are shown. The velocity decreases with volume fraction of nanoparticles due mainly to the increment in nanofluid viscosity. When Reynolds number increases, an increase of both injection from the lower permeable plate and suction at the upper permeable plate is presented. This causes a decrease of the velocity profile and this profile will be skewed towards the upper plate.

Once the velocity field is known, the temperature field for the fluid is determined from the solution of the previous boundary

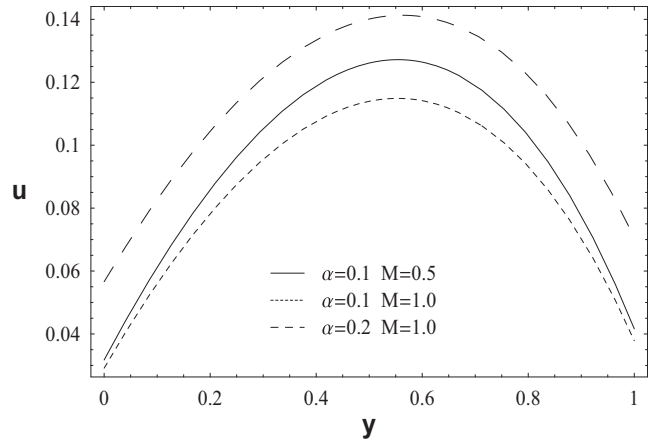


Fig. 2. Velocity profile for different values of α and M . $P = 1, \phi = 0.1, Re = 1$.

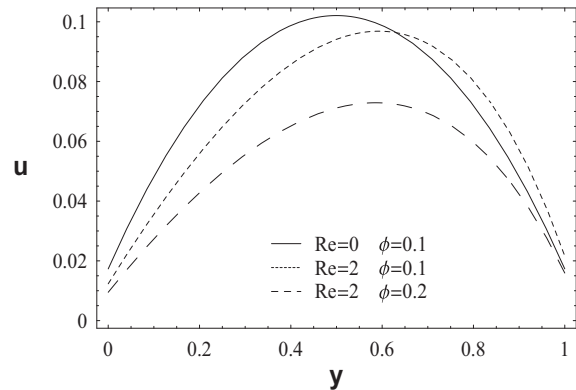


Fig. 3. Velocity profile for different values of Re and ϕ . $P = 1, \alpha = 0.05, M = 1$.

value problem, Eq. (11) under boundary conditions (12 and 13). The analytic result for the temperature profile is

$$\theta(y) = C_3 + C_4 e^{F_6 y}. \tag{20}$$

Here, C_3 and C_4 are function of $P, Re, Bi, Ec, M, \alpha, Pr$ and y . These functions are given by

$$C_3 = \frac{(\rho C)_f Ec}{(\rho C)_{nf} Re} \int \left[\frac{\eta_{nf}}{\eta_f} \left(\frac{du}{dy} \right)^2 + \frac{\sigma_{nf}}{\sigma_f} M^2 u^2 \right] dy + E = \frac{(\rho C)_f Ec}{(\rho C)_{nf} Re} \left(\frac{P^2}{M^2} y + F_{11} + F_{12} \right) + E,$$

$$C_4 = -\frac{(\rho C)_f Ec}{(\rho C)_{nf} Re} \int \left[\frac{\eta_{nf}}{\eta_f} \left(\frac{du}{dy} \right)^2 + \frac{\sigma_{nf}}{\sigma_f} M^2 u^2 \right] e^{-F_6 y} dy + F = \frac{(\rho C)_f Ec}{(\rho C)_{nf} Re} \left(\frac{P^2}{F_6 M^2} e^{-F_6 y} - F_{13} - F_{14} \right) + F.$$

where

$$F_6 = \frac{\left(\frac{k_f}{k_{nf}} \right) \frac{(\rho C)_{nf}}{(\rho C)_f} Pe}{1 + \frac{k_f}{k_{nf}} Rd},$$

$$\left[\frac{\eta_{nf}}{\eta_f} \left(\frac{du}{dy} \right)^2 + \frac{\sigma_{nf}}{\sigma_f} M^2 u^2 \right] = \frac{P^2}{M^2} + e^{\frac{F_1}{2}y} (F_7 \sinh[Ay] + F_8 \cosh[Ay]) + e^{F_1 y} (F_9 \cosh[2Ay] + F_{10} \sinh[2Ay]),$$

$$F_7 = 2PC_1,$$

$$F_8 = 2PC_2,$$

$$F_9 = \left[\left(\frac{\rho_{nf}}{\rho_f} \right)^2 \frac{\eta_f}{\eta_{nf}} \frac{Re^2}{4} + \frac{\sigma_{nf}}{\sigma_f} M^2 \right] (C_1^2 + C_2^2) + \frac{\rho_{nf}}{\rho_f} Re A C_1 C_2,$$

$$F_{10} = 2 \left[\left(\frac{\rho_{nf}}{\rho_f} \right)^2 \frac{\eta_f}{\eta_{nf}} \frac{Re^2}{4} + \frac{\sigma_{nf}}{\sigma_f} M^2 \right] C_1 C_2 + \frac{\rho_{nf}}{\rho_f} \frac{Re}{2} A (C_1^2 + C_2^2),$$

$$F_{11} = \frac{2e^{F_1 y}}{F_1^2 - 4A^2} [(F_1 F_8 - 2AF_7) \cosh[Ay] + (F_1 F_7 - 2AF_8) \sinh[Ay]],$$

$$F_{12} = \frac{e^{F_1 y}}{F_1^2 - 4A^2} [(F_1 F_9 - 2AF_{10}) \cosh[2Ay] + (F_1 F_{10} - 2AF_9) \sinh[2Ay]],$$

$$F_{13} = \frac{2e^{\left(\frac{F_1 - F_6}{2}\right)y}}{(F_1 - 2F_6)^2 - 4A^2} F_{15},$$

$$F_{14} = \frac{e^{(F_1 - F_6)y}}{(F_1 - F_6)^2 - 4A^2} F_{16},$$

$$F_{15} = ((F_1 - 2F_6)F_8 - 2AF_7) \cosh[Ay] + ((F_1 - 2F_6)F_7 - 2AF_8) \times \sinh[Ay],$$

$$F_{16} = ((F_1 - F_6)F_9 - 2AF_{10}) \cosh[2Ay] + ((F_1 - F_6)F_{10} - 2AF_9) \times \sinh[2Ay].$$

The integration constants E and F that appear in the expressions for C_3 and C_4 are solved by the boundary conditions, Eqs. (12) and (13). These constants, that are lengthy and function of $Re, \alpha, M, P, Ec, Pr, Bi, \phi$ and Rd have been generated by making use of the Solve command in Mathematica. Here, the results are similar to those observed in [22]. The temperature of the system near the lower plate is higher than the fluid temperature near the upper plate due to convective heating and hot fluid injection at the lower plate. In all Figures, the values of the fixed parameters are $Re = 1, \alpha = 0.01, M = 0.6, P = Ec = Pr = 1, \phi = 0.1$ and $Rd = 0.8$ while the value of the Biot number is $Bi = 1$ except in Fig. 5 where Biot number is fixed to $Bi = 10$.

Fig. 4 shows effects of volume fraction of nanoparticles, ϕ , and radiation parameter, Rd , on the temperature profile. As ϕ increases, the temperature of the nanofluid in the microchannel increases,

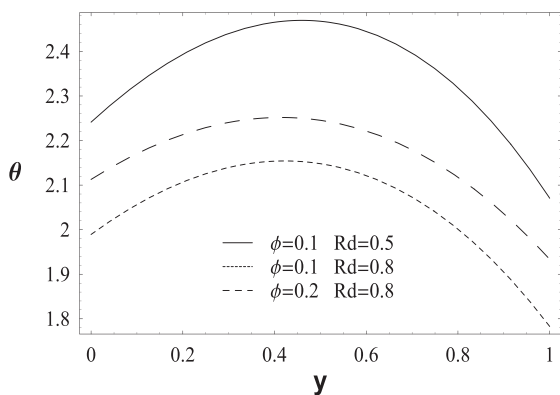


Fig. 4. Temperature profile for different values of ϕ and Rd . $Re = 1, \alpha = 0.01, M = 0.6, P = 1, Ec = 1, Pr = 1, Bi = 1$.

while as Rd increases, the temperature decreases. Fig. 5 shows the influence of Ec and Re numbers on the temperature profile. As Ec number increases, the temperature in the channel increases due to the viscous heating, while as Re number increases, the temperature also increases due mainly to the increase in the injection of hot fluid at the lower porous plate. From Fig. 6, it is observed that increase in Prandtl increases the fluid temperature and increase in Biot number decreases the temperature since the heat transfer to the surroundings is higher. Fig. 7 depicts effects of an increase in both slip flow and Hartmann number on the temperature profile. The temperature of the system decreases with slip

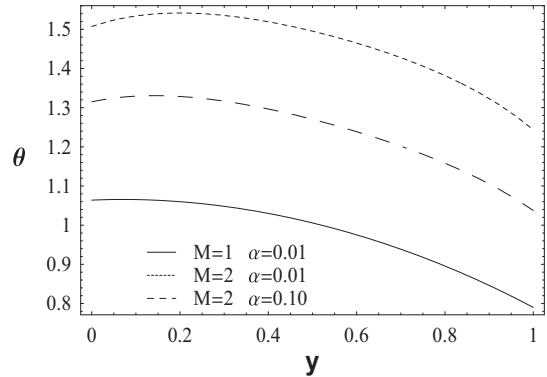


Fig. 5. Temperature profile for different values of M and α . $Re = 1, P = 1, Ec = 1, Pr = 1, \phi = 0.1, Rd = 0.8, Bi = 1$.

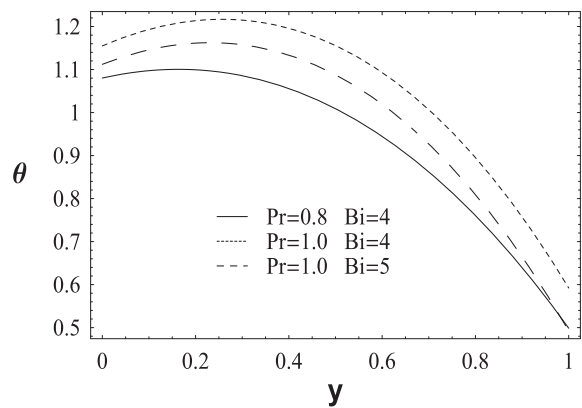


Fig. 6. Temperature profile for different values of Pr and Bi . $Re = 1, \alpha = 0.01, M = 0.6, P = 1, Ec = 1, \phi = 0.1, Rd = 0.8$.

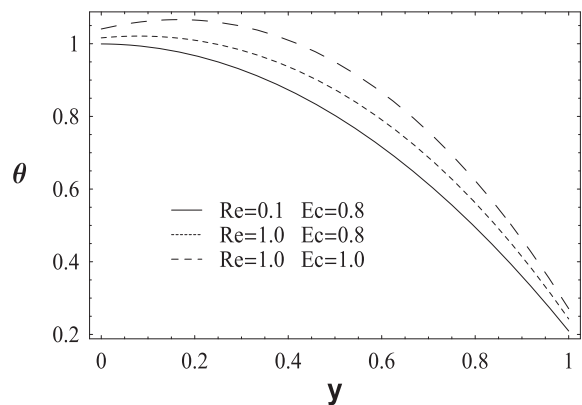


Fig. 7. Temperature profile for different values of Re and Ec . $\alpha = 0.01, M = 0.6, P = 1, Pr = 1, \phi = 0.1, Rd = 0.8, Bi = 10$.

flow since the fluid friction decreases. On the other hand, at high values of Hartmann number (high magnetic field intensity), the temperature of the system increases since the ohmic dissipation in the fluid is higher and this effect dominates over the decrease in the viscous dissipation due to the decrease in the local velocity gradient. Also, when $Bi_1 = Bi_2 \rightarrow \infty$ the temperature profile given by (20) reduces to the expression corresponding to uniform temperature boundary conditions, while the solution of the ordinary non-MHD flow can be obtained in the limit $M \rightarrow 0$ and $Re = 0$. Although, here is not shown, the increase in Reynolds and the decrease in Hartmann and radiation parameter cause a lower increment of the temperature with the volume fraction of nanoparticles.

3. Entropy generation

The velocity and temperature fields already obtained will be used for the determination of the entropy generation rate within the MHD porous microchannel. In flow of a viscous, electrically conducting nanofluid between two porous parallel plates immersed in a magnetic field, entropy generation must consider irreversibilities caused by fluid friction, electric conduction and heat flow. In dimensionless terms, local entropy generation rate can be written explicitly as [26]

$$\dot{S} = \frac{k_{nf}}{k_f} \frac{1}{\Theta^2} \left(\frac{\partial \Theta}{\partial y} \right)^2 + \frac{EcPr}{\Theta} \left[\frac{\eta_{nf}}{\eta_f} \left(\frac{du}{dy} \right)^2 + \frac{\sigma_{nf}}{\sigma_f} M^2 u^2 \right], \quad (21)$$

where \dot{S} is normalized by k_f/a^2 . In Eq. (21), the first term accounts for irreversibilities caused by heat flow in the nanofluid while the second and third terms express local entropy generation due to fluid friction and ohmic dissipation in the nanofluid, respectively. The global entropy generation rate, $\langle \dot{S} \rangle$, is determined by integrating \dot{S} in the whole volume occupied by the microchannel. Once integrated, this quantity only depends on the dimensionless parameters $Re, \alpha, M, P, Ec, Pr, \phi, Rd$ and Bi that govern the performance of the system. In all cases, the dimensionless pressure gradient, P , has been fixed to $P = 1$. Further, due to the small Reynolds and Hartmann numbers in MHD microfluids, their values are chosen lower than or equal to unity ($M = Re \leq 1$) in the majority of cases.

In Fig. 8 the global entropy generation rate is reported as a function of the solid volume fraction of nanoparticles, ϕ , for different values of M and Rd . $Re = 3, \alpha = 0.01, Ec = 1, Pr = 1$ and $Bi = 0.8$. Each curve in Fig. 8 shows that entropy generation reaches minimum values. These minima move to lower values of ϕ when both M and Rd increase. The minimum value of global entropy increases with M and remains approximately constant with Rd . A separate analysis of the different contributions to global entropy generation shows that most of the entropy is generated due to irreversibilities by both heat conduction and viscous dissipation in the nanofluid while the value of ohmic dissipation is lower. Entropy generation produced by heat conduction in the fluid decreases for small values of ϕ due mainly to decrease in the temperature gradient and reaches a minimum value. Once the minimum value is reached, this term exhibits an increase as ϕ grows. On the other hand, the term associated with viscous dissipation in the fluid increases with ϕ due to decrease in the temperature of nanofluid; while the term associated with ohmic dissipation always decreases with ϕ due mainly to decrease in the nanofluid velocity. For small values of ϕ , this reduction in irreversibilities associated with heat conduction and ohmic dissipation dominates over the increment in the term associated with viscous dissipation in the fluid in such a way that global entropy shows a minimum value. In addition, when both M and Rd increase, the increment in the term associated with viscous dissipation in the fluid dominates over the reduction

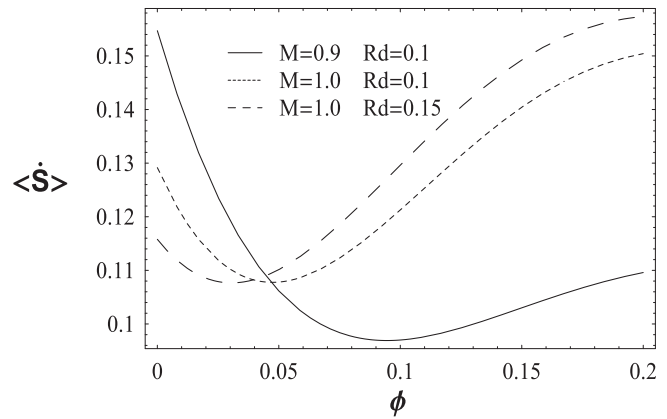


Fig. 8. Global entropy generation as a function of ϕ for different values of M and Rd . $Re = 3, \alpha = 0.01, P = 1, Ec = 1, Pr = 1, Bi = 0.8$.

in the terms associated with heat conduction and ohmic dissipation at lower values of ϕ , therefore the higher the values of M and Rd the lower the optimum value of ϕ where the minimum is reached. It is important to note that for low values of Re ($Re < 1$), the minimum of the term associated with heat conduction disappears and the global entropy generation does not reach a minimum value.

Fig. 9 presents global entropy generation versus radiation parameter, Rd , in the presence of different values of M and ϕ . In addition, $Re = 1, \alpha = 0.01, Ec = 1, Pr = 1$ and $Bi = 1$. Once more, entropy generation reaches minimum values for all curves. When the solid volume fraction of nanoparticles increases the optimum value of the radiation parameter in which entropy generation is minimized remains approximately constant while when the Hartman number increases this value of the optimum radiation parameter decreases.

Fig. 10 shows global entropy generation versus Hartman number, M , for different values of ϕ and Rd . The other parameter values are $Re = 1, \alpha = 0.01, Ec = 1, Pr = 1$ and $Bi = 1$. For each value of ϕ and Rd explored, there is a minimum value for global entropy generation. As the solid volume fraction of nanoparticles, ϕ , increases, this minimum value tends slightly towards lower Hartman numbers while when the radiation parameter increases the optimum value of Hartmann number with minimum entropy moves to lower values. Furthermore, the minimum of global entropy generation when the solid volume fraction of nanoparticles increases attains a lower value.

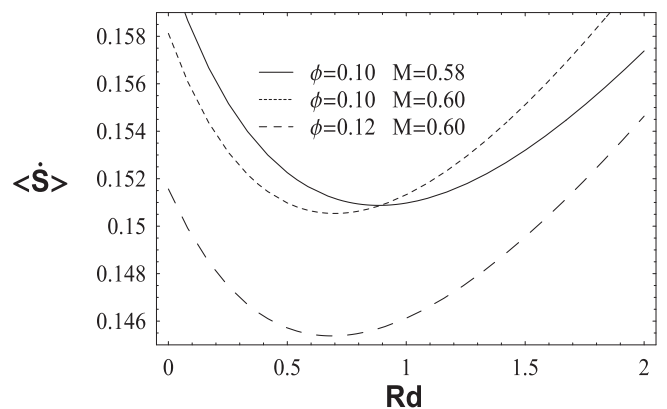


Fig. 9. Global entropy generation as a function of Rd for different values of M and ϕ . $Re = 1, \alpha = 0.01, P = 1, Ec = 1, Pr = 1, Bi = 1$.

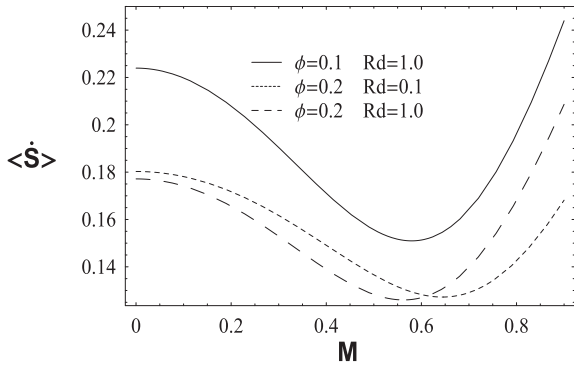


Fig. 10. Global entropy generation as a function of M for different values of Rd and ϕ . $Re = 1, \alpha = 0.01, P = 1, Ec = 1, Pr = 1, Bi = 1$.

In Fig. 11 global entropy generation rate is reported as a function of a single plate slip length (symmetric slip conditions), α , normalized by its value when $\alpha = 0$ for different values of ϕ and Rd . $Re = 1, M = 1, Ec = 1, Pr = 1$ and $Bi = 1$. Optimum operation conditions are obtained for all curves with minimum entropy generation. At higher values of both solid volume fraction of nanoparticles and radiation parameter, the minimum value of global entropy generation occurs at higher value of slip flow.

Fig. 12 shows global entropy generation rate as a function of the Biot number of the lower wall, Bi_1 , for different values of ϕ and Rd . The other parameters are $Re = 1, \alpha = 0.1, M = 0.2, P = 1, Ec = 1, Pr = 1$ and $Bi_2 = 1$. For this case the global entropy generation rate presents a minimum value for two values of ϕ and two values of Rd explored. It is possible to find an optimum Biot number for the lower surface, Bi_{1opt} , which leads to a minimum global entropy generation rate $\langle \dot{S} \rangle$. Here, Joule dissipation in the

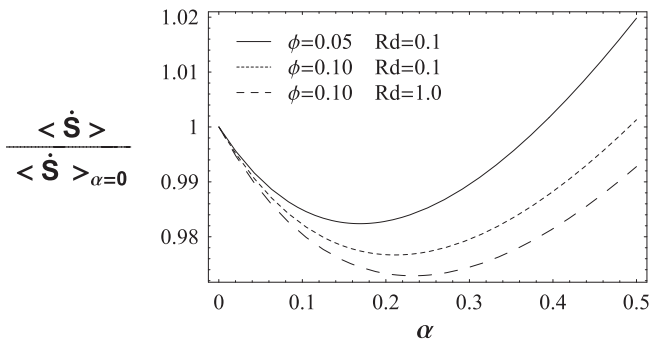


Fig. 11. Normalized global entropy generation as a function of α for different values of Rd and ϕ . $Re = 1, M = 1, P = 1, Ec = 1, Pr = 1, Bi = 1$.

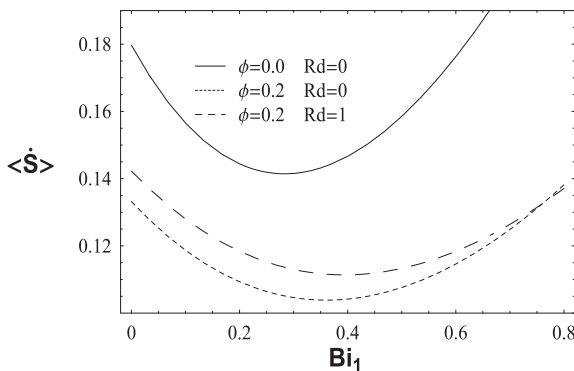


Fig. 12. Global entropy generation as a function of Bi_1 for different values of Rd and ϕ . $Re = 1, \alpha = 0.1, M = 0.2, P = 1, Ec = 1, Pr = 1, Bi_2 = 1$.

fluid is rather small and just leads to a slight decrease in entropy generation rate. When Bi_1 increases, irreversibilities associated with viscous dissipation always increase due to decrease in the fluid temperature promoted by higher heat transfer to the ambient temperature; however, the term associated with dissipation by heat conduction decreases for small values of Bi_1 and reaches a minimum value. This behavior in irreversibilities associated with heat conduction dominates over increase in the term associated with viscous dissipation in such a way that $\langle \dot{S} \rangle$ shows a minimum value. In addition, the higher the value of ϕ the higher the optimum value of $Bi_1; Bi_{1opt}$, where the minimum is reached. The effect of Rd over Bi_{1opt} is not significant. Similar to what was reported in [39,40], we found that when the Biot numbers of each wall are the same (symmetric cooling), global entropy generation rate is always a monotone increasing function of Bi and reaches a limiting value as Bi tends to infinity.

Figs. 13 and 14, show effects of both Prandtl number, Pr , and Reynolds number, Re , on the global entropy generation rate for different values of ϕ and Rd , respectively and $\alpha = 0.01, M = 0.4, Ec = 1$ and $Bi = 2$. In Fig. 13, $Re = 1$, while in Fig. 14, $Pr = 1$. Each curve in both, Figs. 13 and 14, show that global entropy generation rate, $\langle \dot{S} \rangle$, decreases as Pr and Re increase, reaches a minimum and then increases. This means that there is an optimum value of both Pr and Re , that minimizes irreversibilities associated with this system, provided the other parameters remain fixed. These optimum values of Pr and Re , where entropy generation is minimal, increase with both solid volume fraction of nanoparticles and radiation parameter. In Fig. 13, the smallest entropy generation is obtained at the highest value of ϕ , while the effect of Rd on this smallest value of entropy generation is not significant. In Fig. 14, the smallest entropy generation is obtained at the highest values

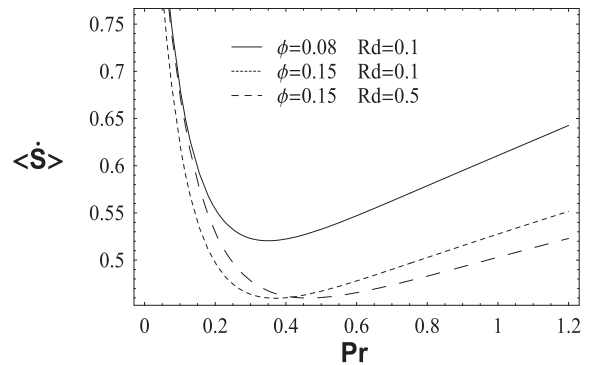


Fig. 13. Global entropy generation as a function of Pr for different values of Rd and ϕ . $Re = 1, \alpha = 0.01, M = 0.4, P = 1, Ec = 1, Bi = 2$.

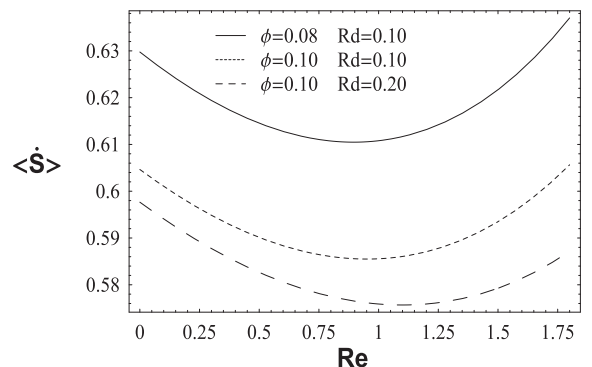


Fig. 14. Global entropy generation as a function of Re for different values of Rd and ϕ . $\alpha = 0.01, M = 0.4, P = 1, Ec = 1, Pr = 1, Bi = 2$.

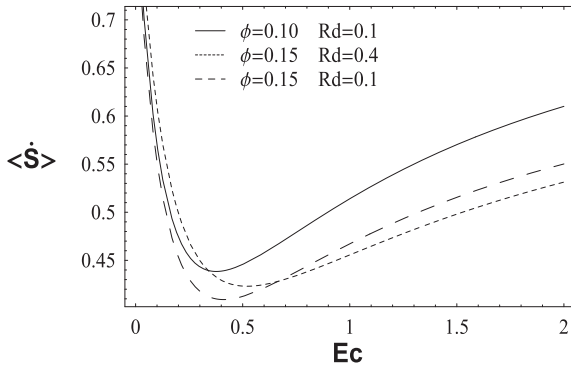


Fig. 15. Global entropy generation as a function of Ec for different values of Rd and ϕ . $Re = 1, \alpha = 0.01, M = 0.5, P = 1, Pr = 1, Bi = 2$.

of both ϕ and Rd . The results obtained for Pr in Fig. 13 are also valid for Peclet number because in this case $Re = 1$ and therefore $Pr = Pe$.

Finally, Fig. 15 shows global entropy generation rate as a function of Eckert number, Ec , at different values of ϕ and Rd when $Re = 1, \alpha = 0.01, M = 0.5, Pr = 1$ and $Bi = 2$. The optimum values of Ec move to highest values when the values of both ϕ and Rd increase. Furthermore, Fig. 15 shows that when ϕ is increased the minimum value of entropy decreases, while this minimum value increases when Rd is increased.

3.1. Nusselt number

The local Nusselt number at the upper wall of the microchannel is given by [41,42]

$$Nu = -\frac{ak_{nf}}{k_f(T_{(y'=a)} - T_b)} \left(\frac{\partial T}{\partial y'} \right)_{y'=a} = -\frac{k_{nf} \left(\frac{d\Theta}{dy} \right)_{y=1}}{k_f (\Theta_{y=1} - \Theta_b)}, \quad (22)$$

where T_b and $T_{(y'=a)}$ are the dimensional expressions of the bulk temperature (i.e. the cross-section averaged temperature of the stream) and the wall temperature at $y' = a$, respectively.

The dimensionless bulk temperature is defined as

$$\Theta_b = \frac{\int_0^1 u \Theta dy}{\int_0^1 u dy}. \quad (23)$$

Fig. 16 shows effect of the volume fraction of nanoparticles, ϕ , on the dimensionless convective heat transfer coefficient, Nu , for different Hartmann numbers. In addition, $Re = 1, \alpha = 0.1, P = 1, Ec = 1, Pr = 1, Rd = 0.1, Bi_1 = 5$ and $Bi_2 = 0.1$. For a given nanofluid and microchannel geometry, changes in M mean variations in the externally applied magnetic field. Results show that for all curves there exists a volume fraction of nanoparticles which leads to maximum heat transfer through the microchannel walls. The behavior observed in the figure indicates that the higher the Hartmann number the higher the maximum value of Nusselt number and the lower the ϕ value where this maximum is reached. Similar behavior is obtained when Nusselt number is plotted versus ϕ for different values of the radiation parameter Rd , namely, maximum values of Nusselt number are obtained for all values of Rd and the higher the radiation parameter, Rd , the higher the maximum value of Nusselt number and the lower the ϕ value where this maximum is reached. In turn, in Fig. 17 the Nusselt number is shown as a function of the Hartmann number for different volume fraction of nanoparticles, while $Re = 0.1, \alpha = 0.1, P = 1, Ec = 1, Pr = 1, \phi = 0.05, Rd = 1, Bi_1 = 2$ and $Bi_2 = 0.1$. Once more, Nu reaches maximum values which correspond to maximum heat transfer. These maximum values of Nusselt become

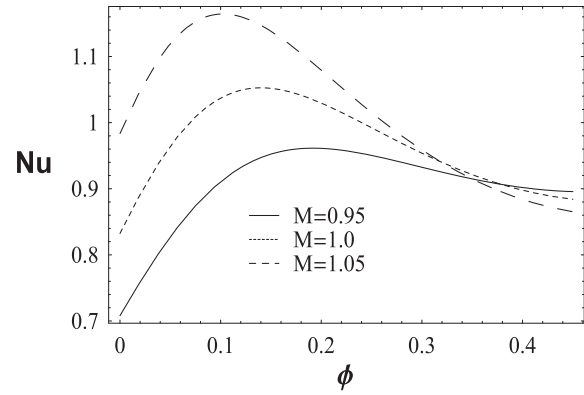


Fig. 16. Nusselt number as a function of the volume fraction of nanoparticles, ϕ , for different Hartmann numbers, M . $Re = 1, \alpha = 0.1, P = 1, Ec = 1, Pr = 1, Rd = 0.1, Bi_1 = 5, Bi_2 = 0.1$.

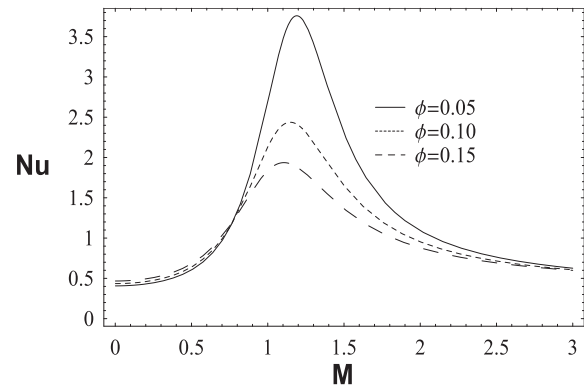


Fig. 17. Nusselt number as a function of Hartmann number, M , for different volume fraction of nanoparticles, ϕ . $Re = 0.1, \alpha = 0.1, P = 1, Ec = 1, Pr = 1, Rd = 1, Bi_1 = 2, Bi_2 = 0.1$.

lower as ϕ increases. The optimum value of M , where the heat transfer is maximum, decreases slightly with the volume fraction of nanoparticles. Although not shown, the Nusselt number is a monotonic increasing function of Rd . The above results are very important in the design of heat exchangers in which maximum heat transfer is required.

4. Summary and conclusion

In this paper we have applied the entropy generation minimization method to the optimization of a water-based Al_2O_3 nanofluid flowing through a porous MHD microchannel with thermal radiation and slip flow. The main objective was to explore combined effects of radiation parameter, hydrodynamic slip, suction/injection, magnetic field, volume fraction of solid nanoparticles and convective boundary conditions on thermal behavior of nanofluid flow, and to show existence of optimal values of these quantities consistent with minimum irreversibilities and maximum heat transfer. Therefore, the novelty of our study was not in the studied configuration but in the obtained results with optimum operation conditions which were not shown in the previous works, and in the analysis of all effects included simultaneously in the model.

It was possible to find optimum values of radiation parameter, nanoparticle volume fraction, Hartmann and Biot numbers which lead to a minimum global entropy generation rate, as well as optimum values of nanoparticle volume fraction and magnetic field strength that maximize the heat transfer. The effects of nanoparticle volume fraction and thermal radiation on the optimum values

of some other parameters were also analyzed. The obtained results showed that optimum values of Biot number, suction/injection Reynolds number, Eckert number and slip flow, where entropy generation was minimum, moved to higher values with both nanoparticle volume fraction and radiation parameter, while optimum values of Hartmann number decreased with both radiation parameter and nanoparticle volume fraction. Also, the minimum values of global entropy, reached in these optimum values of Hartmann, Biot, Eckert and suction/injection Reynolds number, decreased when nanoparticle volume fraction increased. Finally, the Nusselt number, that is, the dimensionless heat transfer coefficient at the walls of the microchannel, was also calculated and analyzed in some specific cases. Optimum values of both Hartmann number and nanoparticle volume fraction that maximize heat transfer were derived.

Although, the linear radiation model was used in the present problem, the obtained results are valid for applications where the values of temperature are not very high and the obtained exact solution might be useful to check the results of other numerical studies on this subject in where more complex radiation models might be studied. The observed trends should also be present in these more complex problems.

The above results are useful in the design of thermal systems such as heat exchangers. Moreover, minimization of global entropy generation that leads to optimal working conditions can be used as a design tool in nanofluid applications, particularly, when electromagnetic interactions are present, as occurs in MHD micropumps.

Acknowledgment

G. Ibáñez thankfully acknowledges financial support from FOMIX-CONACYT (Project 249993).

References

- [1] M. Sheikholeslami, M. Gorji-Bandpy, D.D. Ganji, S. Soleimani, Effect of a magnetic field on natural convection in an inclined half-annulus enclosure filled with Cu-water nanofluid using CVFEM, *Adv. Powder Technol.* 24 (2013) 980–991.
- [2] O. Mahian, S. Mahmud, S.Z. Heris, Analysis of entropy generation between co-rotating cylinders using nanofluids, *Energy* 44 (2012) 438–446.
- [3] M. Torabi, K. Zhang, S. Mahmud, Temperature and entropy generation analyses between and inside rotating cylinders using copper-water nanofluid, *J. Heat Transfer* 137 (2015) 051701 (10 Pages).
- [4] M. Sheikholeslami, D.D. Ganji, Magnetohydrodynamic flow in a permeable channel filled with nanofluid, *Sci. Iran* 21 (2014) 203–212.
- [5] M. Sheikholeslami, M. Gorji-Bandpy, D.D. Ganji, Lattice Boltzmann method for MHD natural convection heat transfer using nanofluid, *Powder Technol.* 254 (2014) 82–93.
- [6] O. Mahian, A. Kianifar, C. Kleinstreuer, M.A. Al-Nimr, I. Pop, A.Z. Sahin, A review of entropy generation in nanofluid flow, *Int. J. Heat Mass Transfer* 65 (2013) 514–532.
- [7] M.J. Uddin, N.H.M. Yusoff, O.A. Bég, A.I. Ismail, Lie group analysis and numerical solutions for non-Newtonian nanofluid flow in a porous medium with internal heat generation, *Phys. Scr.* 87 (2013) 1–14.
- [8] H.A. Mohammed, G. Bhaskaran, N.H. Shuaib, R. Saidur, Heat transfer and fluid flow characteristics in microchannels heat exchanger using nanofluids: a review, *Renew. Sustain. Energy Rev.* 15 (2011) 1502–1512.
- [9] B.H. Salman, H.A. Mohammed, K.M. Munisamy, A.S. Kherbeet, Characteristics of heat transfer and fluid flow in microtube and microchannel using conventional fluids and nanofluids: a review, *Renew. Sustain. Energy Rev.* 28 (2013) 848–880.
- [10] O. Mahian, A. Kianifar, A.Z. Sahin, S. Wongwises, Performance analysis of a minichannel-based solar collector using different nanofluids, *Energy Convers. Manage.* 88 (2014) 129–138.
- [11] C.J. Ho, Y.N. Chung, C.M. Lai, Thermal performance of Al_2O_3 /water nanofluid in a natural circulation loop with a mini-channel heat sink and heat source, *Energy Convers. Manage.* 87 (2014) 848–858.
- [12] T.W. Ting, Y.M. Hung, N. Guo, Effects of streamwise conduction on thermal performance of nanofluid flow in microchannel heat sinks, *Energy Convers. Manage.* 78 (2014) 14–23.
- [13] A.S. Kherbeet, H.A. Mohammed, B.H. Salman, H.E. Ahmed, O.A. Alawi, Experimental and numerical study of nanofluid flow and heat transfer over microscale backward-facing step, *Int. J. Heat Mass Transfer* 79 (2014) 858–867.
- [14] G. Ibáñez, A. López, J. Pantoja, J. Moreira, Combined effects of uniform heat flux boundary conditions and hydrodynamic slip on entropy generation in a microchannel, *Int. J. Heat Mass Transfer* 73 (2014) 201–206.
- [15] G. Ibáñez, A. López, J. Pantoja, J. Moreira, J.A. Reyes, Optimum slip flow based on the minimization of entropy generation in parallel plate microchannels, *Energy* 50 (2013) 143–149.
- [16] O.A. Bég, W.A. Khan, M.J. Uddin, Multiple slip effects on unsteady magnetohydrodynamic nanofluid transport with heat generation/absorption effects in temperature dependent porous media, *J. Porous Media* 18 (9) (2015) 907–922.
- [17] M.J. Uddin, O.A. Bég, A.I. Ismail, Radiative convective nanofluid flow past a stretching/shrinking sheet with slip effects, *J. Thermophys. Heat Transfer* 29 (3) (2015) 513–523.
- [18] A.S. Eegunjobi, O.D. Makinde, Combined effect of buoyancy force and Navier slip on entropy generation in a vertical porous channel, *Entropy* 14 (2012) 1028–1044.
- [19] A.S. Eegunjobi, O.D. Makinde, Effects of Navier slip on entropy generation in a porous channel with suction/injection, *J. Therm. Sci. Technol.* 7 (2012) 522–535.
- [20] T. Chinyoka, Makinde OD analysis of entropy generation rate in an unsteady porous channel flow with Navier slip and convective cooling, *Entropy* 15 (2013) 2081–2099.
- [21] S. Das, R.N. Jana, Entropy generation due to MHD flow in a porous channel with Navier slip, *Ain Shams Eng. J.* 5 (2) (2014) 575–584.
- [22] G. Ibáñez, Entropy generation in MHD porous channel with hydrodynamic slip and convective boundary conditions, *Int. J. Heat Mass Transfer* 80 (2015) 274–280.
- [23] S. Das, A.S. Banu, R.N. Jana, O.D. Makinde, Entropy analysis on MHD pseudo-plastic nanofluid flow through a vertical porous channel with convective heating, *Alexandria Eng. J.* 54 (3) (2015) 325–337.
- [24] M.M. Rashidi, S. Abelman, N.F. Mehr, Entropy generation in steady MHD flow due to a rotating porous disk in a nanofluid, *Int. J. Heat Mass Transfer* 62 (2013) 515–525.
- [25] I. Fersadou, H. Kahalerras, M. El Ganaoui, MHD mixed convection and entropy generation of a nanofluid in a vertical porous channel, *Comput. Fluids* 121 (2015) 164–179.
- [26] C. Zhang, L. Zheng, X. Zhang, G. Chen, MHD flow and radiation heat transfer of nanofluids in porous media with variable surface heat flux and chemical reaction, *Appl. Math. Model.* 39 (1) (2015) 165–181.
- [27] D. Pal, G. Mandal, Hydromagnetic convective–radiative boundary layer flow of nanofluids induced by a non-linear vertical stretching/shrinking sheet with viscous–ohmic dissipation, *Powder Technol.* 279 (2015) 61–74.
- [28] N.V. Ganesh, A.K. Hakeem, R. Jayaprakash, B. Ganga, Analytical and numerical studies on hydromagnetic flow of water based metal nanofluids over a stretching sheet with thermal radiation effect, *J. Nanofluids* 3 (2) (2014) 154–161.
- [29] A. Mushtaq, M. Mustafa, T. Hayat, A. Alsaedi, Nonlinear radiative heat transfer in the flow of nanofluid due to solar energy: a numerical study, *J. Taiwan Inst. Chem. Eng.* 45 (4) (2014) 1176–1183.
- [30] S.K. Nandy, I. Pop, Effects of magnetic field and thermal radiation on stagnation flow and heat transfer of nanofluid over a shrinking surface, *Int. Commun. Heat Mass Transfer* 53 (2014) 50–55.
- [31] M.M. Rahman, W.A. Al-Mazroui, F.S. Al-Hatmi, M.A. Al-Lawatia, I.A. Eltayeb, The role of a convective surface in models of the radiative heat transfer in nanofluids, *Nucl. Eng. Des.* 275 (2014) 382–392.
- [32] M. Habibi Matin, R. Hosseini, M. Simiari, P. Jahangiri, Entropy generation minimization of nanofluid flow in a MHD channel considering thermal radiation effect, *Mechanics* 19 (4) (2013) 445–450.
- [33] M. Mahmoodi, S. Kandelousi, Effects of thermophoresis and Brownian motion on nanofluid heat transfer and entropy generation, *J. Mol. Liquids* 211 (2015) 15–24.
- [34] M. Mahmoodi, S. Kandelousi, Analysis of the hydrothermal behavior and entropy generation in a regenerative cooling channel considering thermal radiation, *Nucl. Eng. Des.* 291 (2015) 277–286.
- [35] M. Torabi, A. Aziz, Entropy generation in a hollow cylinder with temperature dependent thermal conductivity and internal heat generation with convective–radiative surface cooling, *Int. Commun. Heat Mass Transfer* 39 (2012) 1487–1495.
- [36] M. Torabi, K. Zhang, Classical entropy generation analysis in cooled homogenous and functionally graded material slabs with variation of internal heat generation with temperature, and convective–radiative boundary conditions, *Energy* 65 (2014) 387–397.
- [37] M. Torabi, K. Zhang, Heat transfer and thermodynamic performance of convective–radiative cooling double layer walls with temperature-dependent thermal conductivity and internal heat generation, *Energy Convers. Manage.* 89 (2015) 12–23.
- [38] S. Das, R.N. Jana, Entropy generation in MHD porous channel flow under constant pressure gradient, *Appl. Math. Phys.* 1 (3) (2013) 78–89.
- [39] G. Ibáñez, S. Cuevas, M. López de Haro, Minimization of entropy generation by asymmetric convective cooling, *Int. J. Heat Mass Transfer* 46 (14) (2003) 1321–1328.
- [40] G. Ibáñez, S. Cuevas, M. López de Haro, Heat transfer in asymmetric convective cooling and optimized entropy generation rate, *Rev. Mex. Fis.* 49 (2003) 338–343.
- [41] A. Bejan, *Heat Transfer*, John Wiley and Sons, 1993, 675.
- [42] G. Ibáñez, S. Cuevas, Entropy generation minimization of a MHD (magnetohydrodynamic) flow in a microchannel, *Energy* 35 (2010) 4149–4155.





ID	Title	Pages
656340	Entropy generation analysis of a nanofluid flow in MHD porous microchannel with hydrodynamic slip and thermal radiation	9

Related Articles



<http://fulltext.study/journal/673>



-  Categorized Journals
Thousands of scientific journals broken down into different categories to simplify your search
-  Full-Text Access
The full-text version of all the articles are available for you to purchase at the lowest price
-  Free Downloadable Articles
In each journal some of the articles are available to download for free
-  Free PDF Preview
A preview of the first 2 pages of each article is available for you to download for free

<http://FullText.Study>